Journal of Analytical Science and Technology
a SpringerOpen Journal

TECHNICAL NOTE Open Access

Critical importance of the correction of contrast transfer function for transmission electron microscopy-mediated structural biology

Hyeong-Seop Jeong, Hyo-Nam Park, Jin-Gyu Kim and Jae-Kyung Hyun*

Abstracts

Background: Transmission electron microscopy (TEM) is an excellent tool for studying detailed biological structures. High-resolution structure determination is now routinely performed using advanced sample preparation techniques and image processing software. In particular, correction for contrast transfer function (CTF) is crucial for extracting high-resolution information from TEM image that is convoluted by imperfect imaging condition. Accurate determination of defocus, one of the major elements constituting the CTF, is mandatory for CTF correction.

Findings: To investigate the effect of correct estimation of image defocus and subsequent CTF correction, we tested arbitrary CTF imposition onto the images of two-dimensional crystals of Rous sarcoma virus capsid protein. The morphology of the crystal in calculated projection maps from incorrect CTF imposition was utterly distorted in comparison to an appropriately CTF-corrected image.

Conclusion: This result demonstrates critical importance of CTF correction for producing true representation of the specimen at high resolution.

Keywords: Contrast transfer function; Transmission electron microscopy; Electron crystallography; Structural biology

Introduction

Transmission electron microscopy (TEM) offers direct visualization of fine details of biological specimen. Recent advancements in sample preparation techniques and developments in algorithms for sophisticated image processing as well as availability of computation power pivoted rapid improvements in achievable resolution of the analysis and widened the range of biological systems that can be studied (Crowther 2010). In particular, structural analysis of protein macromolecules by TEM, either in the form of ordered arrays such as protein two-dimensional (2D) crystals or individual protein macromolecules, has improved greatly as evidenced by an increasing number of structure determination at near-atomic resolutions (Armache et al. 2010; Ge and Zhou 2011; Gonen et al. 2005; Yu et al. 2011). In addition, TEM analysis of biological system at moderate resolution can directly complement high-resolution structures obtained by X-ray crystallography and nuclear magnetic resonance (NMR) spectroscopy, providing pseudo-atomic resolution structure determination of large, multi-subunit complexes.

One of the key factors for successful structure determination of a biological specimen at high resolution is the correction for contrast transfer function (CTF) of a microscope. While images obtained from the electron microscope suffers from loss of faithful representation of the true object due to phase and amplitude modulation derived from imperfect imaging conditions, CTF models how an electron microscope transfers the actual specimen into a recorded image hence allowing for distortions present in the micrograph to be estimated (Frank 2006). Under weak-phase approximation, that is, electron scattering and the subsequent phase shift, is small as in the case for biological specimen, TEM image, and CTF can be described by the following relationships (Penczek et al. 1997):

$$I(k) = H(k)\Phi(k) \quad (1)$$

* Correspondence: hjk002@kbsi.re.kr
Division of Electron Microscopic Research, Korea Basic Science Institute, 169-148 Gwahangno, Daejeon 305-333, Republic of Korea

$$H(k) = \sin\gamma(k) - W\cos\gamma(k) \quad (2)$$

where k is the spatial frequency vector, $I(k)$ is Fourier transform of micrograph, $\Phi(k)$ is Fourier transform of true object and $H(k)$ is CTF. W is amplitude contrast ratio, which denotes contribution of image contrast that result from inelastic scattering in the image formation that is dominated by elastic electron scattering, and $\gamma(k)$ is phase shift produced by spherical aberration and defocus that can be described by the Scherzer formula (Williams and Carter 1996),

$$\gamma(k) = \frac{\pi}{2}\left(C_s\lambda^3k^4 - 2\Delta z\lambda k^2\right) \quad (3)$$

where k is the scattering vector, λ is the wavelength of electron beam, Cs is the spherical aberration coefficient of a microscope, and Δz is the defocus value. While other parameters are constant for a given instrument, defocus is manually adjusted by an operator in order to produce image with optimal phase contrast. When considering elastic electron scattering alone, $\sin\gamma(k)$ is also referred to as phase contrast transfer function (PCTF). When plotted as a function of spatial frequency, PCTF oscillates sinusoidally, hence producing alternating negative phase contrast at higher spatial frequencies (Ruprecht and Nield 2001). If the negative contrast is left uncorrected, structural features of the object at high resolution is compromised, and therefore the image fails to represent true features of the object.

Additional complication with regard to precise CTF estimation comes from continuous attenuation of amplitude towards higher spatial frequency, termed envelope function, which is described by a simplified relationship below:

$$H(k) = E(k)H_{\text{ideal}}(k) \quad (4)$$

where the experimental CTF, $H(k)$, results from ideal CTF, $H_{\text{ideal}}(k)$, multiplied by envelope function, $E(k)$. Major contributors of envelope function include beam energy envelope (E_{spread}), beam coherence envelope ($E_{\text{coherence}}$) and sample drift envelope (E_{drift}). Each envelope function is described by complex formula which takes account into parameters such as chromatic aberration of the microscope, semi-angle of aperture, energy spread of emitted beam, lens current stability and specimen drift (Frank 2006; Sorzano et al. 2007). In addition, the performance of image recorder, as defined by modulation transfer function, also contributes to the degradation of high-resolution information in the micrograph.

Due to its importance, there have been a significant number of studies dedicated to precisely determine CTF from micrographs. These works provided comprehensive description and algorithms for specific aspects such as defocus determination (Mindell and Grigorieff 2003), amplitude contrast (Toyoshima and Unwin 1988; Toyoshima et al. 1993) and envelope function (Saad et al. 2001; Sander et al. 2003) as well as generation of reliable power spectrum density (Fernandez et al. 1997; Zhu et al. 1997) from which CTF of experimental data can be modeled from. As a result, CTF correction is now widely incorporated in various image processing software packages, and routinely performed for structure determination of vitrified biological specimen.

In the present work, the effect of precise estimation of image defocus, one of the most critical parameters required for CTF determination, in the preservation of structural integrity of specimen is demonstrated. Although the effects of alterations in critical parameters have been thoroughly investigated for CTF determination in the past (Sorzano et al. 2009), the main purpose of this short technical note is to illustrate visually the effect of appropriate CTF correction. Therefore, for simplicity, detailed theories of image formation in TEM and algorithms employed in CTF correction are omitted.

Availability and requirements

Specimen preparation and electron microscopy

2D crystals of Rous sarcoma virus (RSV) capsid protein with C-terminal truncation mutation ($CA_{1\text{-}226}$) was produced using mild acidification as described previously (Bailey et al. 2012; Hyun et al. 2010). In short, purified protein stored in low molarity buffer at neutral pH was jump-diluted with high molarity buffer at pH 4.9, followed by a 48-h incubation at 18°C.

Five microliters of the assembly product was applied onto a glow-discharged grid that was held by self-closing, anti-capillary tweezers (EMS, Hatfield, PA, USA). 60 to 90 s were allowed for the specimen to be adsorbed onto the carbon support film. Excess salt was washed off using three droplets of filtered, deionized water. Then, 5 μL of 2% (*w/v*) uranyl acetate solution was applied onto the grid. After staining for 60 s, excess stain solution was blotted away using a piece of filter paper.

A Tecnai 12 TEM (FEI, Hillsboro, OR, USA) equipped with lanthanum hexaboride (Lab_6) gun operating at 120 kV was used to acquire images of $CA_{1\text{-}226}$ 2D crystals. The images were recorded on SO-163 photographic films (Kodak, Rochester, NY, USA) at nominal magnification of ×42,000, at approximately 1.5 μm under-focus. The films were developed in D19 developer (Kodak, USA) diluted 1:1 (*v/v*) with water for 10 min.

Image processing

Micrographs that displayed minimal astigmatism and drift were scanned using a Super Coolscan 9000 film scanner (Nikon, Tokyo, Japan). The micrographs were digitized at a step size of 10.0 μm (i.e., 2,549 dpi), which corresponded to 2.38 Å/pixel on the specimen. Within

the micrograph, 2,048 × 2,048 pixel box that displayed best crystalline order was cropped for image processing.

2dx program suite was employed for image processing of the 2D crystals (Gipson et al. 2007a, b). The overall process of image processing is summarized in Figure 1. Fourier transform of the micrograph was used to determine lattice parameters by assigning each diffraction spot with Miller index. Also, astigmatism and defocus of the image was estimated using the CTFFIND3 software (Mindell and Grigorieff 2003) that is implemented in 2dx. For correct estimation of image defocus, spherical aberration of the microscope (2 mm), acceleration voltage (120 kV) and amplitude contrast for negatively stained specimen (20% contribution) were provided. Inherent distortions and imperfection of the raw image was corrected using unbending routine, which employs cross-correlation between a small reference area and the rest of the image (Crowther et al. 1996). Background noise from Fourier transform was eliminated by masking diffraction spots, and inverse Fourier transformation was performed in order to produce noise-filtered image. Prior to the generation of a projection map from the noise-filtered and unbent data, CTF was corrected using Weiner filtering, based on the estimated defocus and astigmatism. For a given defocus value, CTF was simulated using the ctfExplorer software (Sidorov 2002). Instrumental parameters for appropriate CTF simulation were estimated by comparing computed intensity profile

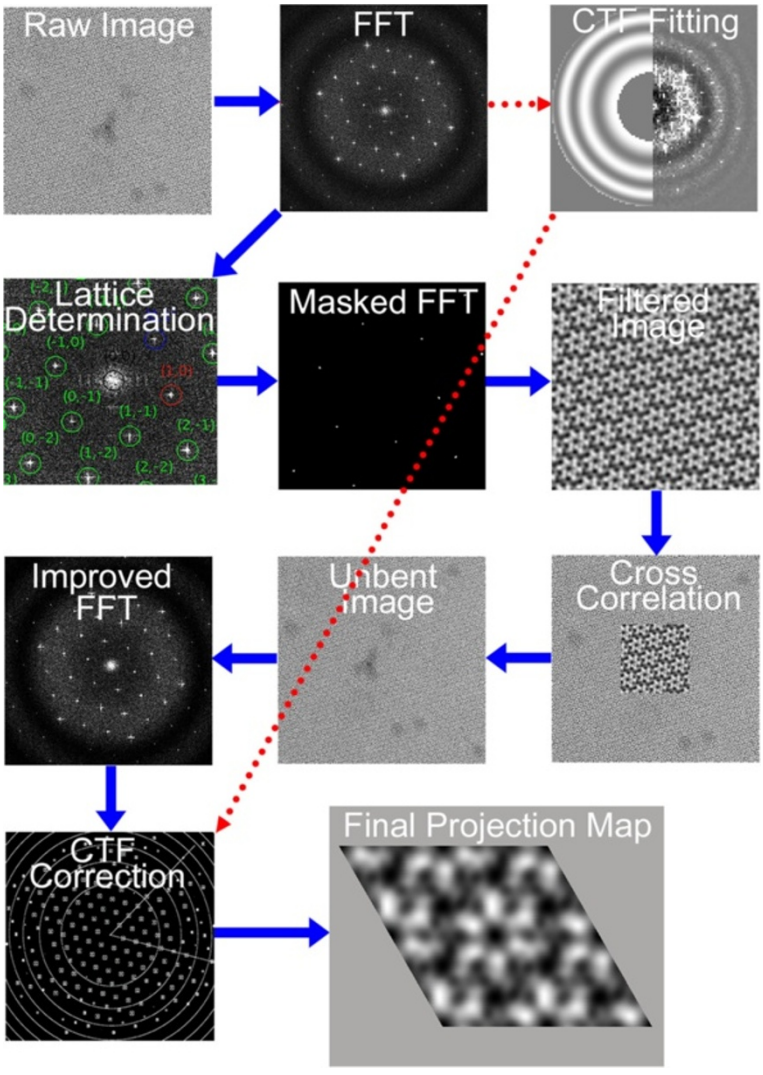

Figure 1 Overview of image processing of a 2D crystal. Raw electron micrograph is Fourier transformed, from which unit cell parameter for the crystal lattice is determined. Fourier transform (FFT) is also used to determine image defocus and CTF fitting. Diffraction spots from FFT are masked in order to eliminate background noise. A filtered image that results from inverse Fourier transformation of masked FFT serves as a reference for cross-correlation-based image unbending. FFT from unbent image is CTF-corrected, and final projection image is generated by inverse Fourier transform.

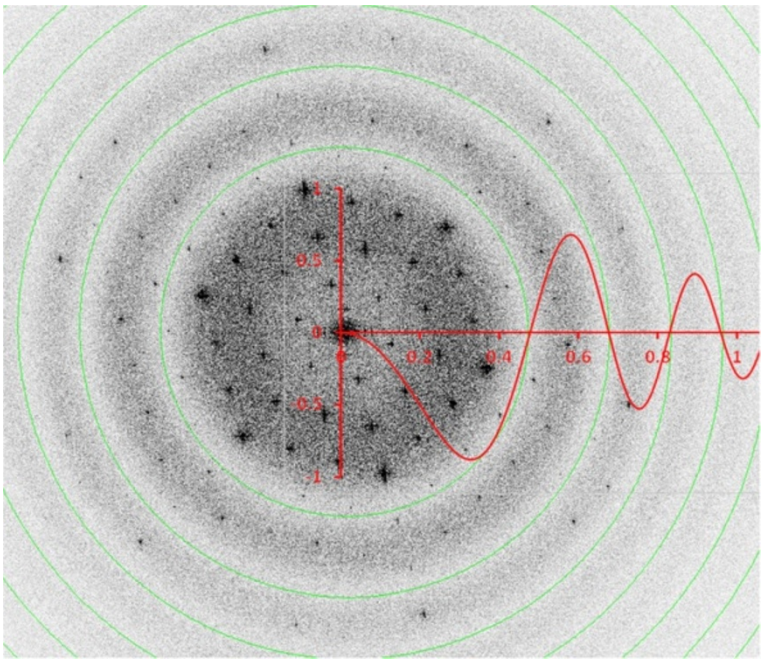

Figure 2 CTF fitted Fourier transform of RSV CA 2D crystal. FFT of RSV $CA_{1\text{-}226}$ 2D crystal clearly indicates Thorn rings that represent CTF plotted as a function of spatial frequency (red graph). Positions of zero CTF are indicated by green circles in the image. Diffraction spots that belong in every second Thorn rings in the FFT (i.e. positive CTF in the plot) must be phase-flipped in order to correctly extract information to a highest possible resolution.

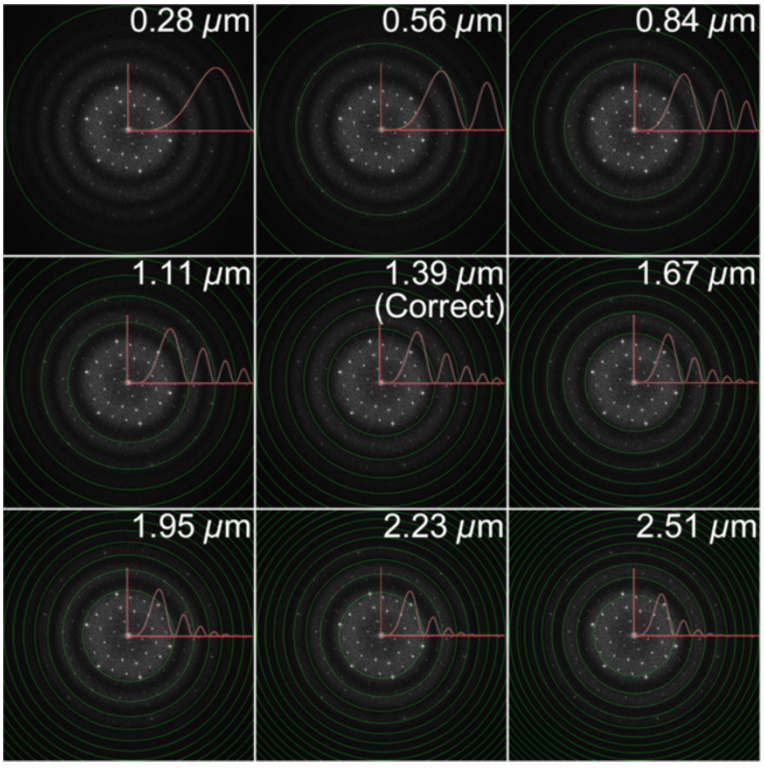

Figure 3 Fitting of arbitrary CTFs to the Fourier transform of RSV CA 2D crystal. CTFs derived from arbitrary defocus values are fitted onto FFT of RSV CA 2D crystal. Positions of calculated zero CTF are indicated by green circles in the image, and clear misfit is observed when the wrong CTF is fitted. Simulated CTF (red graph) was plotted based on the absolute values (i.e., intensity profile mode) for the simplicity.

obtained from a radial average of experimental Fourier transform with the calculated simulation. Satisfactory agreement between the experimental data and the simulation was achieved using 0.26 mrad convergence angle, 14.3 nm focal spread and, 2 eV energy spread. Subtle astigmatism in the image was not taken account into for the simulation.

Findings

Raw electron micrograph of RSV $CA_{1\text{-}226}$ 2D crystal exhibited hexagonal lattice symmetry with hexameric subunits clearly defined. Fourier transform of the image displayed amplitude modulation in the form of Thorn ring that represents CTF, and the diffraction spots extended far beyond the first node of CTF, up to approximately 14 Å. Estimation of defocus indicated that that the image was slightly astigmatic, where defocus of the image was estimated to be 13,917 and 13,447 Å in the longest and shortest dimensions that are perpendicular. Fitted CTF is shown in Figure 2, in which an independently simulated CTF function is overlaid. Correctly estimated defocus in the image enabled precise positioning of minimal CTF in the Fourier transform, and the simulated CTF indicates oscillating positive and negative CTF as a function of resolution as well as resolution-dependent attenuation of phase amplitude. The plot indicates necessity for phase correction to diffraction spots (i.e., structure factors) that belong in every second node of Thorn rings.

Lattice parameters in reciprocal space were obtained by indexing diffraction spots, from which real space unit cell dimension was calculated (a = 96.203 Å, b = 96.385 Å, and γ = 119.964°). Initial phase and amplitude were extracted from unique reflections of h and k Miller indices in the Fourier transform. In order to distinguish diffraction from the 2D crystal from random background noise in the Fourier transform, the quality of the structural information was measured in terms of 'intelligence quotient (IQ)' number, where the signal-to-noise ratio of the reflection from the background is determined. IQ = 1 indicates signal-to-noise ratio of 8, whereas IQ = 9 is undistinguished spot from background. After initial structure

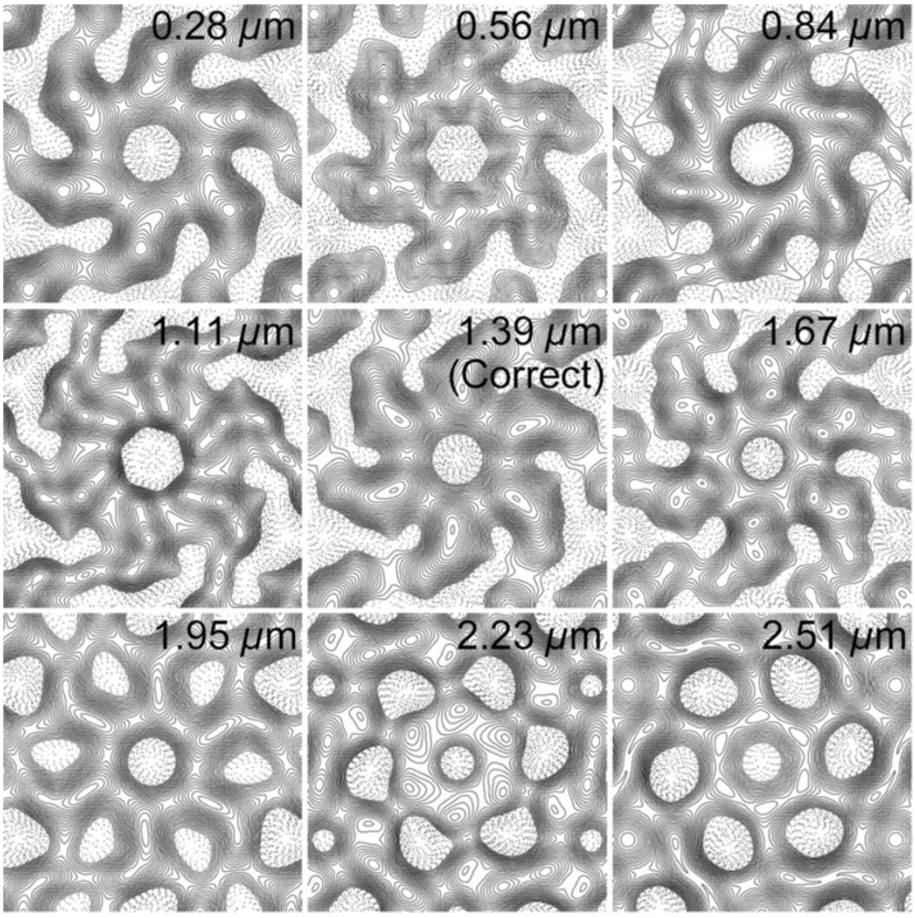

Figure 4 Projection maps resulting from wrong CTF fitting. Projection maps were produced from the data that had been fitted with arbitrary CTF (Figure 3). Structural alterations from the correct structure are apparent, although the degree of deformation varies between the maps.

factor extraction from diffraction spots with IQ score higher than 3 (good spots), filtered image was generated. Then, using a small area of the filtered image as a reference, lattice distortions in the whole image was corrected through cross-correlation between the reference and the whole image. After the unbending process, the number of 'good spots' increased from initial data by 194%.

In order to characterize the effect of CTF correction on the preservation of structural integrity, the data was either corrected for CTF from estimated defocus, or by applying arbitrary defocus values (Figure 3). For both CTF-corrected data and the data that was processed with incorrect CTF estimation, symmetry of the lattice was searched from one of 17 possible plain group symmetries. Phase residual in all cases was the lowest (28°) for p6, which agreed well with visual inspection of raw electron micrograph. Based on the symmetry, phase origin of the image was determined, and then projection maps with p6 symmetry imposition were generated (Figure 4).

Projection map of CTF-corrected image exhibited RSV CA hexamer with a central cavity, and weak density connection that links neighboring hexamers. In contrast, some projection maps produced from incorrect CTF imposition exhibited drastically altered structure. The degree of structural alteration was most dramatic when π/2 phase shift from the correct CTF was imposed, causing local phase contrast reversal in the structure (2.23 and 2.51 μm under-focus in Figure 3). In particular, such phase reversal at lower spatial frequency (resolution) compromised overall shape of the protein, leading to a complete misrepresentation of the actual specimen. Also, rapid attenuation of amplitude of those images, as shown by simulated CTF plots (red graphs in Figure 3), resulted in the loss of high-resolution structural features in the projection maps. Incorrect phase reversal at spatial frequency higher than the first node of CTF (0.56 and 0.84 μm under-focus in Figure 3) resulted changes in detailed features above approximately 20 Å resolution, of which close inspection of the structure or side-by-side comparison with known reference (i.e., atomic model) must be carried out in order to ensure structural integrity. When no phase correction was performed within the resolution limit of the data (0.28 μm in Figure 2), structural deformation of final map was subtle although the density distribution within the map varied significantly from the correct map.

As shown in the simulated CTF, it is to be noted that the attenuation of signal at higher spatial frequency changes significantly depending on the image defocus due to envelope function. Since envelope function is directly related to CTF, signal attenuates more rapidly at higher defocus (Zhou and Chiu 1993). Therefore, optimization of image defocus is necessary in order to capture high-resolution details up to a potential information limit of a given electron microscope, while producing enough image contrast for weak phase objects such as vitrified biological specimen. Such optimization, which may be based on simulated CTF or by trial-and-error, can be omitted when using highly coherent beam source such as field emission gun since the envelope function is greatly improved and amplitude attenuation is reduced at the resolution range that is adequate for structural analysis at molecular level (Zhou and Chiu 1993). In addition, development of phase plate may displace need for CTF correction for high-resolution imaging because the device allows for in-focus images with high image contrast (Nagayama 2011).

Conclusions

Structure determination of protein macromolecules using TEM is advancing rapidly, both in the range of applications and in the achievable resolution. Development of image processing algorithms made major contribution in such a rapid growth, and estimation of correct defocus and CTF correction played essential role for extending the resolution of the analysis. In this technical note, the importance of correct image defocus, a key parameter for CTF determination, was addressed through a simple image processing experiment. By illustratively demonstrating drastic misinterpretation of true structural features that result from wrong CTF correction, this study is expected to guide researchers, especially the beginners in the field, for careful monitoring of image processing steps in order to extract high resolution structural data.

Competing interests

The authors declare that they have no competing interests.

Authors' contributions

HJK designed and coordinated the study. HSJ and PHN carried out experiments and image processing. HJK, JHS and JGK refined the data, and drafted the manuscript. All authors read and approved the final manuscript.

Acknowledgements

This work was supported by the Korea Basic Science Institute grant (T33518) to J-K Hyun.

Received: 22 June 2013 Accepted: 2 September 2013
Published: 16 Sep 2013

References

Armache JP, Jarasch A, Anger AM, Villa E, Becker T, Bhushan S, Jossinet F, Habeck M, Dindar G, Franckenberg S, Marquez V, Mielke T, Thomm M, Berninghausen O, Beatrix B, Söding J, Westhof E, Wilson DN, Beckmann R (2010) Cryo-EM structure and rRNA model of a translating eukaryotic 80S ribosome at 5.5-A resolution. Proc Natl Acad Sci USA 107(46):19748–19753

Bailey GD, Hyun JK, Mitra AK, Kingston RL (2012) A structural model for the generation of continuous curvature on the surface of a retroviral capsid. J Mol Biol 417(3):212–223

Crowther RA (2010) From envelopes to atoms: the remarkable progress of biological electron microscopy. Adv Protein Chem Struct Biol 81:1–32

Crowther RA, Henderson R, Smith JM (1996) MRC image processing programs. J Struct Biol 116(1):9–16

Fernandez JJ, Sanjurjo J, Carazo JM (1997) A spectral estimation approach to contrast transfer function detection in electron microscopy. Ultramicroscopy 68:267–295

Frank J (2006) Three-dimensional electron microscopy of macromolecular assemblies. Oxford University Press, New York
Ge P, Zhou ZH (2011) Hydrogen-bonding networks and RNA bases revealed by cryo electron microscopy suggest a triggering mechanism for calcium switches. Proc Natl Acad Sci USA 108(23):9637–9642
Gipson B, Zeng X, Stahlberg H (2007a) 2dx_merge: data management and merging for 2D crystal images. J Struct Biol 160(3):375–384
Gipson B, Zhang ZY, Stahlberg H (2007b) 2dx–user-friendly image processing for 2D crystals. J Struct Biol 157(1):64–72
Gonen T, Cheng Y, Sliz P, Hiroaki Y, Fujiyoshi Y, Harrison SC, Walz T (2005) Lipid-protein interactions in double-layered two-dimensional AQP0 crystals. Nature 438(7068):633–638
Hyun JK, Radjainia M, Kingston RL, Mitra AK (2010) Proton-driven assembly of the Rous Sarcoma virus capsid protein results in the formation of icosahedral particles. J Biol Chem 285(20):15056–15064
Mindell JA, Grigorieff N (2003) Accurate determination of local defocus and specimen tilt in electron microscopy. J Struct Biol 142(3):334–347
Nagayama K (2011) Another 60 years in electron microscopy: development of phase-plate electron microscopy and biological applications. J Electron Microsc (Tokyo) 60(Suppl 1):S43–S62
Penczek PA, Zhu J, Schröder R, Frank J (1997) Three dimensional reconstruction with contrast transfer compensation from defocus series. Scanning Microsc 11:147–154
Ruprecht J, Nield J (2001) Determining the structure of biological macromolecules by transmission electron microscopy, single particle analysis and 3D reconstruction. Prog Biophys Mol Biol 75(3):121–164
Saad A, Ludtke SJ, Jakana J, Rixon FJ, Tsuruta H, Chiu W (2001) Fourier amplitude decay of electron cryomicroscopic images of single particles and effects on structure determination. J Struct Biol 133(1):32–42
Sander B, Golas MM, Stark H (2003) Automatic CTF correction for single particles based upon multivariate statistical analysis of individual power spectra. J Struct Biol 142(3):392–401
Sidorov MV (2002) CtfExplorer: interactive software for 1d and 2d calculation and visualization of TEM phase contrast transfer function. Microsc Microanal 8:1572–1573
Sorzano CO, Jonic S, Núñez-Ramírez R, Boisset N, Carazo JM (2007) Fast, robust, and accurate determination of transmission electron microscopy contrast transfer function. J Struct Biol 160(2):249–62
Sorzano CO, Otero A, Olmos EM, Carazo JM (2009) Error analysis in the determination of the electron microscopical contrast transfer function parameters from experimental power Spectra. BMC Struct Biol 9:18
Toyoshima C, Unwin N (1988) Contrast transfer for frozen-hydrated specimens: determination from pairs of defocused images. Ultramicroscopy 25(4):279–291
Toyoshima C, Yonekura K, Sasabe H (1993) Contrast transfer for frozen-hydrated specimens II: amplitude contrast at very low frequencies. Ultramicroscopy 48:165–176
Williams DB, Carter CB (1996) Transmission electron microscopy: a textbook for material science. Plenum Press, New York
Yu X, Ge P, Jiang J, Atanasov I, Zhou ZH (2011) Atomic model of CPV reveals the mechanism used by this single-shelled virus to economically carry out functions conserved in multishelled reoviruses. Structure 19(5):652–61
Zhou ZH, Chiu W (1993) Prospects for using an IVEM with a FEG for imaging macromolecules towards atomic resolution. Ultramicroscopy 49(1–4):407–416
Zhu J, Penczek PA, Schröder R, Frank J (1997) Three-dimensional reconstruction with contrast transfer function correction from energy-filtered cryoelectron micrographs: procedure and application to the 70S Escherichia coli ribosome. J Struct Biol 118(3):197–219

10.1186/2093-3371-4-14
Cite this article as: Jeong *et al.*: Critical importance of the correction of contrast transfer function for transmission electron microscopy-mediated structural biology. *Journal of Analytical Science and Technology* 2013, 4:14